



Substitution of Ca^{2+} in Calcite by Sn^{2+} and Sr^{2+} cations through ion exchange characterized by X-ray absorption and photoelectron spectroscopies

Jonathan B. Junio^{1,2} · Prae Chirawatkul³ · Marlon T. Conato² · Candy C. Mercado¹

Received: 19 December 2020 / Accepted: 10 April 2021 / Published online: 20 April 2021
© The Author(s) 2021

Abstract

Tin (Sn^{2+}) and strontium (Sr^{2+}), two potential alternatives to lead (Pb^{2+}) in perovskite formation, were explored in transforming calcium carbonate (CaCO_3) into a leaving group in a cation exchange reaction. This is the first part of a sequential ion exchange process in transforming calcite into a Pb-free perovskite material for perovskite solar cell applications. Calcite, a polymorph of CaCO_3 , was successfully transformed into strontianite (SrCO_3) through a cation exchange reaction. In the Sn substitution reaction on the other hand, no SnCO_3 formation was noted. Instead, oxides of Sn were formed. The wider spaces in between Ca^{2+} cations in (100) orientation account for the higher atomic Sn^{2+} and Sr^{2+} concentrations as compared to (001) orientation, where the cation movement is restricted. X-ray absorption and photoelectron spectroscopies were used to investigate the ion-exchange transformation of calcite towards the formation of an intermediate carbonate material.

Introduction

Calcite, the most stable polymorph of calcium carbonate (CaCO_3) at most temperatures and pressures, is an important and dominant component of marine sediments [1]. Trace elements present in it had been used as indicators in different fields of research such as a record of past climate conditions, particularly seawater temperatures [2]. The incorporation of Sr^{2+} in calcite has also helped understand biomineralization and age determination of marine limestones [3].

In this study, the substitution of Ca^{2+} cations was explored as the first part of a sequential ion exchange process in transforming calcite into a Pb-free perovskite material for PSC applications. Transforming various types of metal carbonate structures into lead halide perovskite materials was already reported [4]. The transformation was achieved

through a two-step ion exchange process by first introducing lead ions (Pb^{2+}) and replacing calcium (Ca^{2+}) and second, by using as a leaving group the CO_3^{2-} anion, facilitating ion exchange with halide ions, followed immediately by methylammonium (MA) insertion to form the perovskite material ($\text{CH}_3\text{NH}_3\text{PbX}_3$). In this study, the resulting materials were characterized through modern techniques and several factors affecting the ion exchange process defined. However, factors behind the ion exchange process were not investigated. There is still a need to understand the influence of immersion time and material properties such as crystal orientation to the rate of ion exchange. Ionic adsorption on various planar surfaces of muscovite [5], kaolinite [6] and calcite [7] had been studied through molecular dynamics simulations. However, the rate at which Sn^{2+} and Sr^{2+} ions are diffused in calcite at (100) and (001) orientations were not explored in these simulations nor in experiments. In this study, reactions for both Sn^{2+} and Sr^{2+} were investigated for both (100) and (001) orientations.

The cation exchange to convert calcite to cerussite or lead carbonate (PbCO_3), the first step in the two-step ion exchange process, was already carried out in a previous study [8]. The study was primarily aimed at the sequestration of Pb^{2+} into bulk calcite through dissolution/ crystallization to address Pb^{2+} contamination in groundwater aquifers and soils. In this study, the local environments of the incoming cations Sn^{2+} and Sr^{2+} —which are Pb^{2+} alternatives, as the

✉ Jonathan B. Junio
jbjunio4@up.edu.ph

¹ Department of Mining, Metallurgical and Materials Engineering, University of the Philippines, Diliman, 1101 Quezon City, Philippines

² Institute of Chemistry, University of the Philippines, Diliman, 1101 Quezon City, Philippines

³ Synchrotron Light Research Institute, Nakhon Ratchasima, Thailand

bulk calcite material is transformed, were explored. X-ray absorption, and photoelectron spectroscopies were used to investigate the ion-exchange transformation of single-crystal calcite towards the formation of an intermediate carbonate material.

For a successful cation exchange taking place, some requirements were put forward [9]. First, there should be higher mobility for the outgoing cation, which means a smaller ionic radius. The ionic radii of Pb²⁺ (1.19 Å), Sn²⁺ (1.22 Å), Sr²⁺ (1.18 Å) and Ca²⁺ (1.00 Å) based on Shannon's work [10] are nearly identical with Ca²⁺ having the smallest—or highest mobility. Second, the outgoing cation (Ca²⁺) solubility should be higher than that of the incoming cation, as indicated by the solubility product constant (K_{sp}). The K_{sp} of Ca²⁺ is higher than those of Pb²⁺ and Sr²⁺ [11]. Third, the lattice energy of the final crystal should be less than the original crystal. The lattice energies, U of the incoming crystal cations Pb²⁺ and Sr²⁺ are less than that of the outgoing cation Ca²⁺ [12].

Materials and methods

Materials

Single-crystal CaCO₃ (100) and (001) orientations, 10×10×0.5 mm, polished (MTI), Strontium nitrate ACS reagent ≥ 99% and Tin (II) sulfate ≥ 95% (Sigma Aldrich).

CaCO₃ single crystals to SnCO₃/SrCO₃ conversion

CaCO₃ single crystals were cleaved into irregular shapes and placed on scintillation bottles with the polished surface facing up. Each bottle was filled with 20 ml of either SnSO₄ or Sr(NO₃)₂ 0.5 M solutions. Low pressure (LP) samples were immersed for 4 h at 250 mbar and continued for the next 20 h at atmospheric pressure (AP). The Sr and Sn samples for the 8/16/24 h study were capped loosely and set aside at atmospheric pressure and room temperature (30 °C). The crystals were immersed in deionized water for 24 h to stop the conversion reaction, washed with deionized water, immersed in acetone for 1 h, and allowed to air dry for 30 min.

Experimental methods

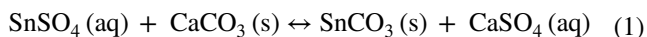
The XAS at BL1.1 W: Multiple X-ray Techniques station has a double crystal monochromator (DCM) using Si (111), and available photon energy range of 4 to 18 keV and beam size at sample position (H×V) of 5 mm×2.5 mm. The XPS at BL5.3 uses a PHI5000 Versa probe II (ULVAC-PHI, Japan) equipped with a hemispherical electron energy analyzer. The excitation source is a monochromatic Al K α X-ray

gun (1486.6 eV). The binding energy of all XPS spectra was calibrated with the C1s peak at 284.8 eV.

Results and discussion

Sn²⁺ → Ca²⁺ cation exchange

Below Eq. (1) shows the expected transformation of CaCO₃ immersed in a SnSO₄ solution to form stannous carbonate:



X-ray absorption spectroscopy (XAS) was used to determine the local environment of Sn in the cation exchange-treated single crystal calcite. For this sample, the Sn spectra were taken at the Sn L-edge at 4465 eV. One way to compare Sn100_LP with references is to inspect the fine structures before the white line at the vicinity of the Sn L₃ edge of the two and compare the difference (Δ) of the three weak peaks (red and blue lines) as shown in Fig. 1. The Δ values of Sn100_LP, 9.8, and 12.5 eV are comparable to the SnO Δ values of 11 and 11.3 eV from the SLRI standard and the study of Liu et al. [13] (11.1 and 11.4 eV). These results mean that Sn100_LP is more similar to SnO than SnO₂ and, therefore, leans to an oxidation state of 2+ instead of 4+.

X-ray photoelectron spectroscopy (XPS) was used to analyze the surface chemistry of the resulting materials. Table 1 summarizes the atomic concentration of Ca²⁺ and Sn²⁺ for the Sn → Ca samples at different immersion times. Three samples are of the same orientation (100), concentration, and subjected to immersion times of 8, 16, and 24 h while a 4th sample from each set has a (001) orientation immersed for 24 h at atmospheric pressure and room temperature.

The atomic concentration of the incoming cation (Sn²⁺) increased with increasing immersion time. This increase is indicative of the rise in the number of cations exchanged as a function of time. Consequently, the Ca²⁺ %Atom decreased with increasing immersion time, an indication of the amount of Ca²⁺ transformed. The %Atom for Sn100_24 is higher as compared to Sn001_24—21.41 versus 6.04%.

The atomic concentrations and the Gaussian multi-peak fitting spectra of both Sn3d_{5/2} and Ca2p are shown in Fig. 2. For Sn3d_{5/2}, the atomic concentrations of (100) and (001)—21.41 and 6.04%, respectively, align with the peak heights of the XPS spectra (Fig. 2c to d), with much higher peaks for (100) at 3d_{5/2} = 485 eV, 3d_{3/2} = 493.41 eV with Δ = 8.41 eV [14]. As expected, it is the opposite in the case of Ca2p, as shown in Fig. 2a and b. From Fig. 2c, (100)'s 3d_{5/2} = 487 eV closely corresponded with tin dioxide (SnO₂) while that of Fig. 2d (001), 3d_{5/2} = 486.34 eV, with that of SnO.

XPS spectra in the region of Sn3d_{5/2}, showed the composition of Sn3d_{5/2} in terms of Sn (metal) and Sn (oxide). In

Fig. 1 The fine structure in the vicinity of the Sn L_3 edge of SnO_2 , SnO and Sn on Sn100_LP (Sn sample with (100) orientation)

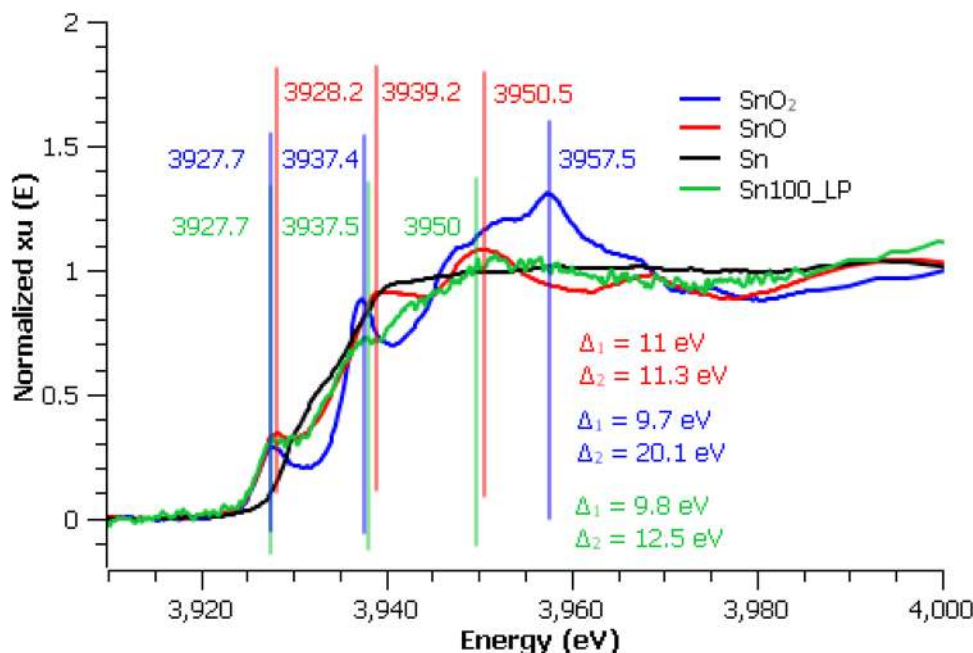


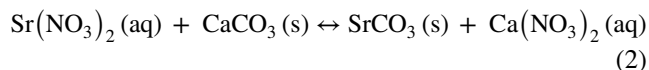
Table 1 Atomic concentration of key elements from XPS narrow scan of Sn^{2+} and Sr^{2+} samples

Solution	Sample code	Atomic concentration (%)	
		Ca2p	Sn3d5
SnSO_4	Sn100_8	14.25	1.34
	Sn100_16	7.51	16.64
	Sn100_24	5.2	21.41
	Sn001_24	11.04	6.04
Solution	Sample code	Atomic concentration (%)	
		Ca2p	Sr3d
$\text{Sr}(\text{NO}_3)_2$	Sr100_8	12.14	0.08
	Sr100_16	10.02	0.15
	Sr100_24	7.03	1.34
	Sr001_24	9.21	0.89

Fig. 2e and f, the content is mostly Sn oxide as compared to the low Sn metal content. Although the Sn metal content cannot be further broken down into SnO_2 and SnO oxides in XPS, the results confirm the XAS findings on the presence of these oxides, with both techniques showing the more dominant presence of SnO as compared to SnO_2 .

$\text{Sr}^{2+} \rightarrow \text{Ca}^{2+}$ cation exchange

Strontium is also regarded as one of the most promising alternatives according to the Goldschmidt's rules and quantum mechanical analysis [15]. The ionic radius of Sr^{2+} and Pb^{2+} are nearly identical [10], implying that the substitution won't greatly affect the crystal structure. Below Eq. (2) shows the expected calcite to strontianite transformation:



Sr spectra for XAS were taken at the Sr K-edge at 16,105 eV. The white line peak positions, E of samples Sr100_LP and Sr001_LP are 16,122 and 16,123 eV, respectively, which are closer to the reference SrCO_3 value of 16,126 eV as compared to the strontium oxide (SrO) value of 16,128 eV (Fig. 3). The values of E vary across references such as that of $\text{SrCO}_3 = 16,112$ eV [16] and 16,119 eV [17] while for SrO , it is 16,120 eV [17] and 16,104 eV [18]. For this reason, the data are presented as measured and compared to values of the reference samples measured on the same time frame.

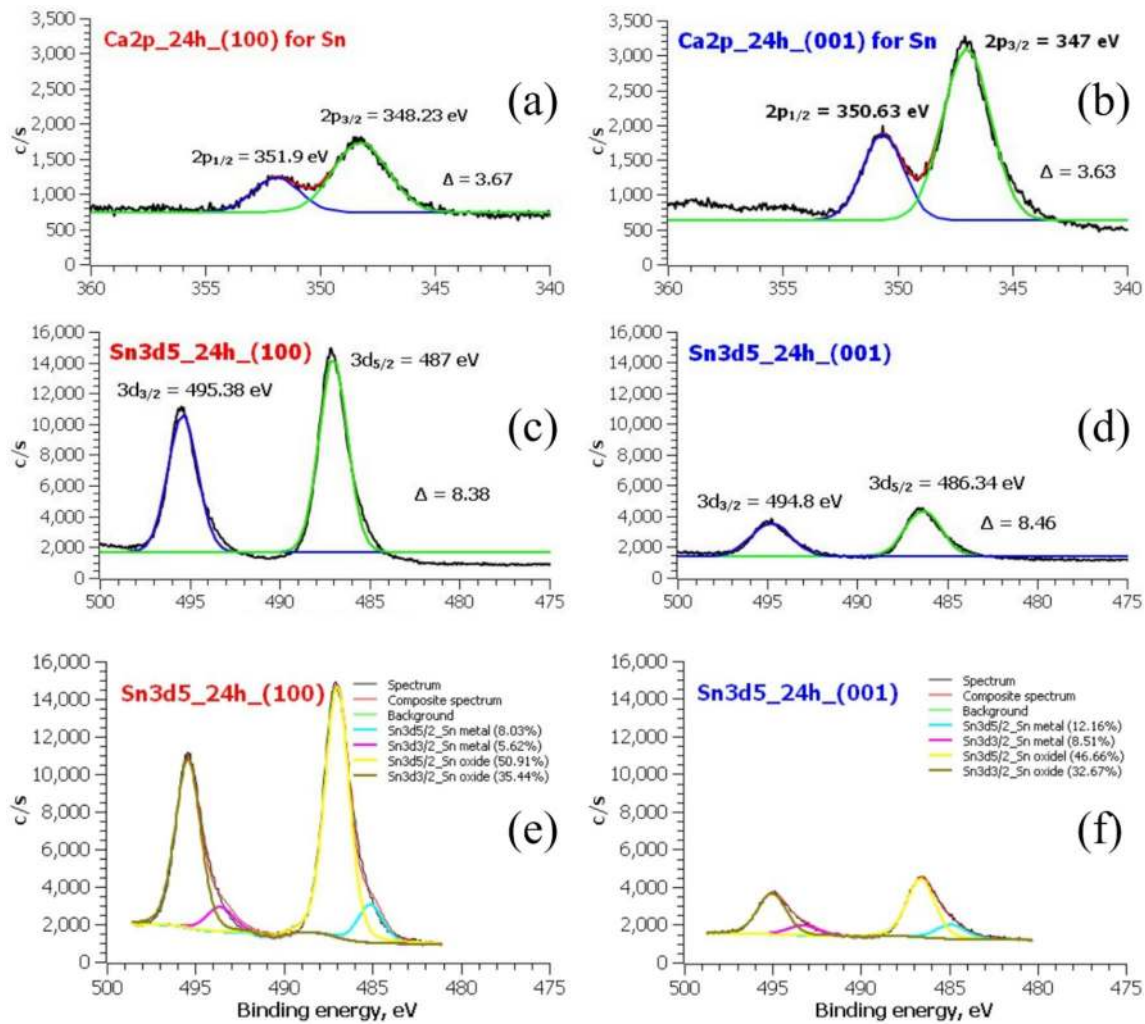


Fig. 2 Element specific XPS narrow scan spectra for **a** Ca2p (100) vs. **b** (001) orientations and **c** Sn3d5 (100) vs. **d** (001) orientations. Element specific XPS narrow scan spectra after curve fitting for **e** Sn3d5 (100) vs. **f** (001) orientations

The absence of doublet typical in calcite or Sr in calcite can also be observed for both (100) and (001) samples. The doublet noted on both calcite and Sr in calcite in previous studies [16, 19] occur at 4048 and 4060 eV peaks. This absence means that the local structure of Sr in the samples at a probe depth of 1–2 μm is in the carbonate structure of SrCO_3 and not calcite nor Sr in calcite. The SrCO_3 local structure means that there is no (or very thin) interface between the calcite and strontianite layers.

For XPS, the atomic concentration of the incoming Sr^{2+} cation increased while the Ca^{2+} %Atom decreased with increasing immersion time. The %Atom for Sr100_24 is higher as compared to Sr001_24—1.34 versus 0.89%.

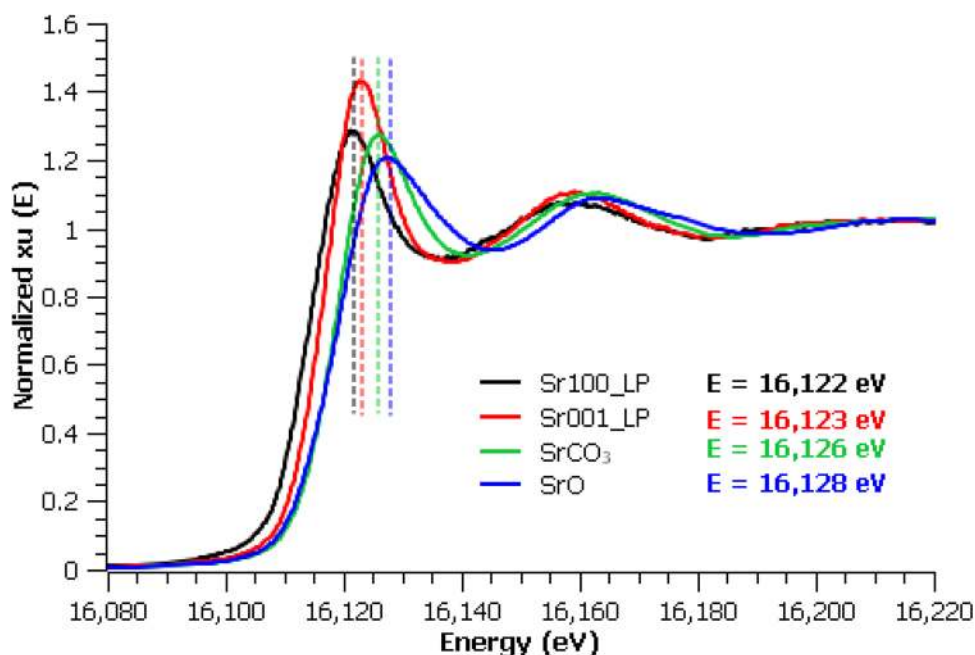
The atomic concentrations of both Sr3d and Ca2p are also shown in Table 1, compared in terms of the starting material calcite's orientation: (100) or (001). For Sr3d, the atomic concentration between (100) and (001)—1.34 and 0.89%, respectively, aligns with the peak heights of the XPS

spectra (Fig. 4c, d), with much higher peaks for (100). As in the case of Sn, it is the opposite for Ca2p, as shown in Fig. 4a and b. From the same reference [14], the values are: $3d_{5/2} = 134.3$ eV, $3d_{3/2} = 136.09$ eV with $\Delta = 1.79$ eV. From Fig. 4c, (100)'s $3d_{5/2} = 133.78$ eV and that of Fig. 4d (001), $3d_{5/2} = 133.67$ eV are more aligned with that of strontianite.

The XPS spectra in the region of Sr3d after curve fitting are shown in Fig. 4e and f. Here, the composition of Sr3d is mostly SrCO_3 . These results confirm the XAS findings on the successful CaCO_3 to SrCO_3 transformation.

To compare (100) and (001) orientations for calcite, crystallographic images at viewing directions (100) and (001) are shown in Fig. 5. The top figures show both orientations with the direction of diffusion perpendicular to this orientation. The figures show varying distances between cations from 3.3 to 4.7 \AA for (100) orientation which means that the rate of cation exchange is faster due to wider spaces available for the interacting ions to move around. The same is not

Fig. 3 Sr K-edge X-ray Absorption Near-Edge Structure (XANES) for single crystal samples with (100) and (001) orientations after Sr cation exchange with reference samples SrCO_3 and SrO



true for (001), where Ca^{2+} ions are adjacent to each other, restricting movement. The difference in orientation accounts for the higher atomic Sn and Sr concentrations for (100) orientation as compared to (001) as shown in Table 1. This anisotropic property of calcite had been demonstrated in helium (He) diffusion [20], where diffusivities in calcite cut in c-perpendicular direction were about two orders of magnitude lower than for those in the c-parallel direction and normal to cleavage faces, even though the diffusion activation energies for both are comparable. The reason for this is that all minerals show larger limiting inter-atomic apertures along the c-parallel than along the c-perpendicular direction. Also, the degree of anisotropy can be attributed to the magnitude of the aperture difference. For example, as compared with the other trigonal minerals: dolomite and magnesite, calcite is the most anisotropic diffusion-wise—with a 20% difference between the smallest maximum apertures along the [100] and [001] axes, which are 1.2 Å and 1.0 Å, respectively. Ionic porosity, defined as the percentage of its unit-cell volume not occupied by ions, was also put forward as an influence to diffusion rate as these unoccupied spaces offer pathways for diffusing ions. The linear relationship between diffusivity and ionic porosity had been demonstrated in the

study of both Pb^{2+} and Sr^{2+} diffusion in calcite and other minerals [21].

Conclusion

Calcite to strontianite transformation was confirmed by both XAS and XPS. Sr samples with (100) and (001) orientations showed the absence of a typical doublet in the XAS spectra indicating that the local structure of Sr in the samples is in the carbonate structure of SrCO_3 and not calcite nor Sr in calcite. The atomic concentration for both the incoming cations (Sn^{2+} and Sr^{2+}) increased with increasing immersion time. Instead of forming SnCO_3 , the cation exchange resulted in Sn, mostly in the form of oxides, as shown in XPS. The Sn oxides were found to be more of SnO than SnO_2 based on the delta (Δ) of the three peaks of the Sn sample under XAS. There are wider spaces available for Ca^{2+} cations in (100) orientation while the cations are adjacent to each other in (001) orientation, restricting movement. This difference in ionic spacing of the two orientations accounts for the higher atomic Sn and Sr concentrations for (100) as compared to (001) orientation.

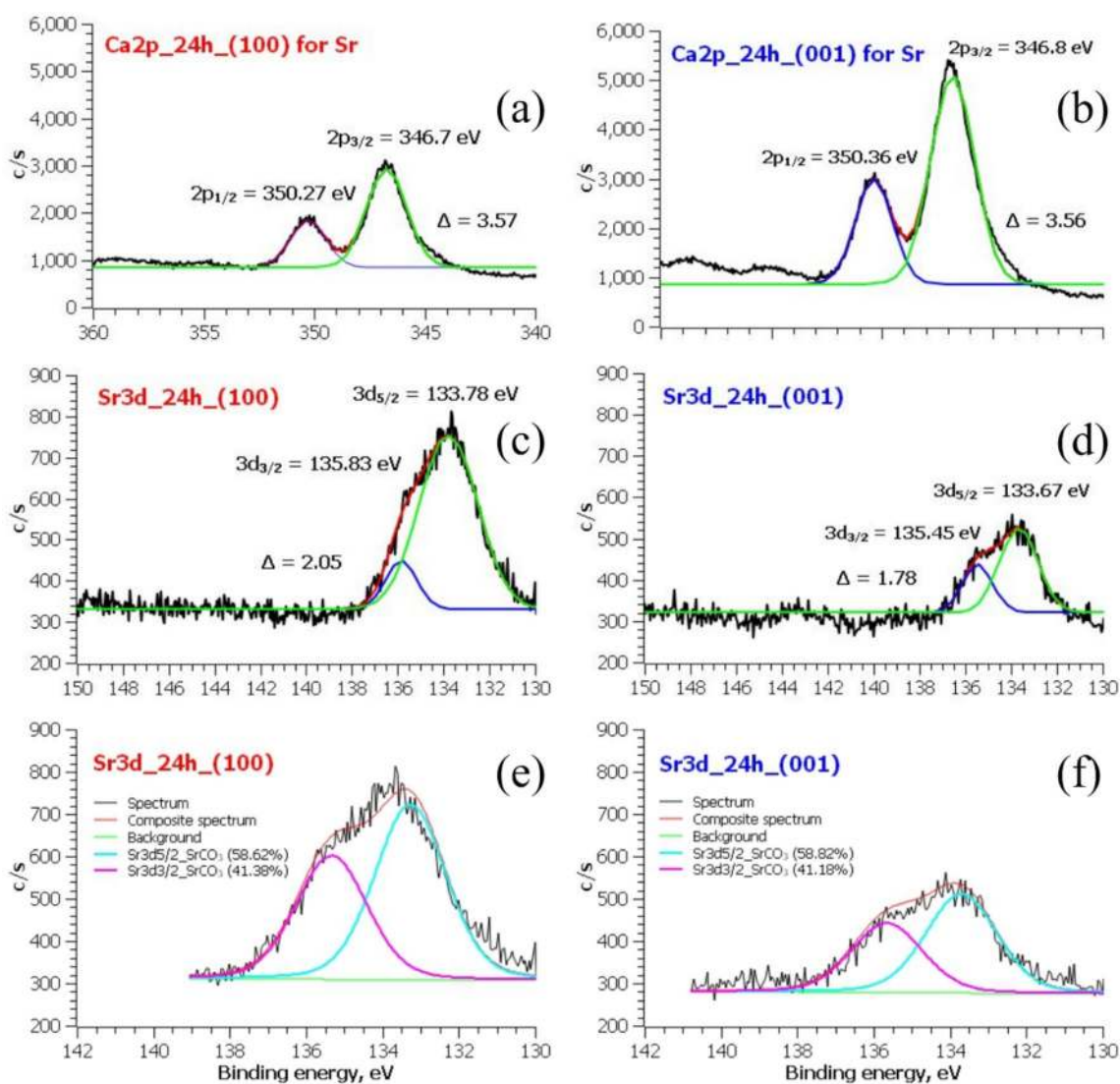
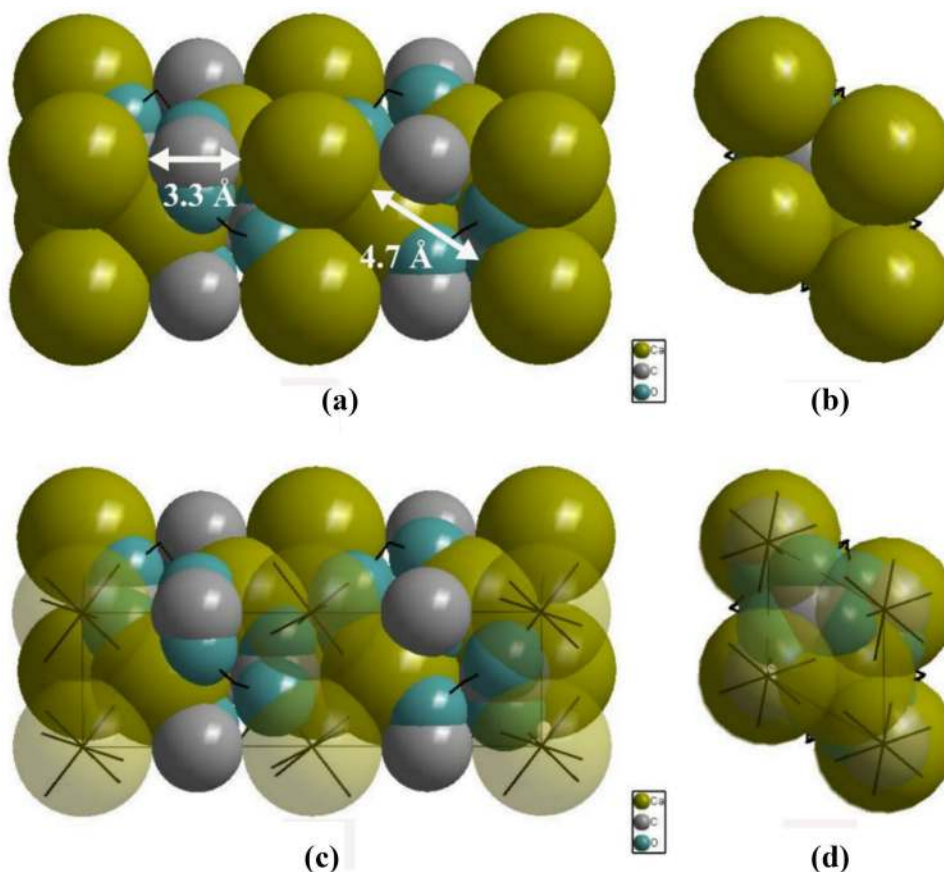


Fig. 4 Element specific XPS narrow scan spectra for **a** Ca2p (100) vs. **b** (001) orientations and **c** Sr3d (100) vs. **d** (001) orientations. Element specific XPS narrow scan spectra after curve fitting for **e** Sr3d (100) vs. **f** (001) orientations

Fig. 5 Crystallographic image of calcite at (100) and (001) orientations [22]: **a** calcite (100) and **b** calcite (001) space-filling image viewed perpendicular to orientation (with dimensions), **c** calcite (100) and **d** calcite (001) space-filling image viewed perpendicular to orientation (with front atoms made transparent)



Acknowledgements This work was funded by a grant under the Engineering Research and Development for Technology (ERDT) of the Philippine Department of Science and Technology (DOST). The XAS and XPS characterizations were made possible under beamtime application ID # 6006: BL1.1W: Multiple X-ray techniques and ID # 5855: BL5.3 SLRI X-ray Photoelectron Spectroscopy (XPS), respectively. These were performed at the Synchrotron Light Research Institute (SLRI), Nakhon Ratchasima, Thailand.

Data availability The data that support the findings of this study are available from the corresponding author upon request.

Declaration

Conflict of interest On behalf of all authors, the corresponding author states that there is no conflict of interest.

Open Access This article is licensed under a Creative Commons Attribution 4.0 International License, which permits use, sharing, adaptation, distribution and reproduction in any medium or format, as long as you give appropriate credit to the original author(s) and the source, provide a link to the Creative Commons licence, and indicate if changes were made. The images or other third party material in this article are included in the article's Creative Commons licence, unless indicated otherwise in a credit line to the material. If material is not included in the article's Creative Commons licence and your intended use is not permitted by statutory regulation or exceeds the permitted use, you will need to obtain permission directly from the copyright holder. To view a copy of this licence, visit <http://creativecommons.org/licenses/by/4.0/>.

References

1. J.W. Morse, R.S. Arvidson, *Chem. Rev.* **107**, 342–381 (2007)
2. G.A. Gaetani, A.L. Cohen, *Geochim. Cosmochim. Acta.* **70**, 4617–4634 (2006)
3. W.H. Burke, R.E. Denison, E.A. Hetherington, R.B. Koepnick, H.F. Nelson, J.B. Otto, *Geology* **10**, 516–519 (1982)
4. T. Holtus, L. Helmbrecht, H. C. Hendrikse, I. Baglai, S. Meuret, G. W. Adhyaksa, E. C. Garnett, W. L. Noorduyn, *Nat. Chem.* **2018**, 1–6.
5. N. Loganathan, A.G. Kalinichev, *J. Phys. Chem. C* **121**, 7829–7836 (2017)
6. W. Yang, A. Zaoui, *Appl. Clay Sci.* **80–81**, 98–106 (2013)
7. S. Bai, J. Kubelka, M. Piri, *J. Mol. Liq.* **2021**, 1–9.
8. K. Yuan, S.S. Lee, V. De Andrade, N.C. Sturchio, P. Fenter, *Environ. Sci. Technol.* **50**, 12984–12991 (2016)
9. J.B. Rivest, P.K. Jain, *Chem. Soc. Rev.* **42**, 89–96 (2013)
10. R.D. Shannon, *Acta Cryst. A* **32**, 751–767 (1976)
11. J. A. Dean, *Lange's Handbook of Chemistry*. (New York: McGraw-Hill, Inc., 1999), pp. 8.8, 8.11, 8.15.
12. W.M. Haynes, *CRC Handbook on Chemistry and Physics* (CRC Press Taylor & Francis Group, Boca Raton, 2017), pp. 12–23
13. Z. Liu, K. Handa, K. Kaibuchi, Y. Tanaka, J. Kawai, *JESRA* **135**, 155–158 (2004)
14. J. F. Moulder, W. F. Stickle, S. E. Peter, K. D. Bomben, J. Chastain, *Handbook of X-ray Photoelectron Spectroscopy*. (Minnesota: Perkin-Elmer Corporation, 1992), pp. 69, 105, 127.
15. T.J. Jacobsson, M. Pazoki, A. Hagfeldt, T. Edvinsson, *J. Phys. Chem. C* **119**, 25673–25683 (2015)
16. A.A. Finch, N. Allison, *Mineral. Mag.* **71**, 539–552 (2007)

17. T.-L. Chou, T.-S. Chan, J.-M. Chen, H. Yamauchi, M. Karpinen, J. Solid State Chem. **202**, 27–32 (2013)
18. A. Sharma, M. Varshney, W. Cheol Lim, H.-J. Shin, J. P. Singh, S. O. Won, K. H. Chae, *Phys. Chem. Chem. Phys.* 2017, 1–9.
19. R.B. Gregor, N.J.E. Pingitore, F.W. Lytle, *Science* **275**, 1452–1454 (1997)
20. D.J. Cherniak, W. Amidon, D. Hobbs, E.B. Watson, *Geochim. Cosmochim. Acta.* **165**, 449–465 (2015)
21. Z.-F. Zhao, Y.-F. Zheng, *Am. Mineral.* **92**, 289–308 (2007)
22. K. Brandenburg, H. Putz, M. Berndt. (Diamond, 2019), <http://www.crystalimpact.com/company.htm>. Accessed 1 October 2019.